

# **Sound Speed Estimation from Sparse Environmental Measurements with Application to Mode Filtering**

**Eric R. St. Pierre and Kathleen E. Wage**

September 2005

*Proceedings of the 2005 IEEE/MTS Oceans Conference, Vol. 2,  
pp. 1345-1351.*

© 2005 IEEE. Personal use of this material is permitted. However, permission to reprint/republish this material for advertising or promotional purposes or for creating new collective works for resale or redistribution to servers or lists, or to reuse any copyrighted component of this work in other works must be obtained from the IEEE.

# Sound Speed Estimation from Sparse Environmental Measurements With Application To Mode Filtering

Eric R. St. Pierre and Kathleen E. Wage

Electrical and Computer Engineering Department, George Mason University

**Abstract-** Acoustic mode filtering requires accurate knowledge of the mode shapes and wavenumbers at the receiver, which are functions of the sound speed profile. During a year-long deployment, environmental measurements, hence measurements of sound speed, often consist of data from a small set of temperature sensors mounted on the vertical receiving array. This paper describes a space-time Kalman filter framework for estimating the sound speed profile from a spatially-sparse set of temperature measurements. The approach assumes that the changes in sound speed associated with slow variations in the environment can be written in terms of the quasi-geostrophic dynamic modes. The paper analyzes the sound speed errors associated with the method and considers how those errors propagate through the mode computations. Examples using environmental measurements made during the North Pacific Acoustic Laboratory experiment are provided.

## I. INTRODUCTION

Mode filtering of underwater acoustic receptions depends on accurate knowledge of the mode shapes and wavenumbers. The acoustic modes are the eigenfunctions of the ocean waveguide derived from the Helmholtz equation. Given the sound speed profile (SSP), standard algorithms can be used to solve a Sturm-Liouville problem to yield the mode shapes and wavenumbers. Difficulties arise when the SSP is not known exactly. Inaccuracies in the profile lead to errors in the shape and wavenumber computations, which result in mismatch between the mode filter and the received signals. From an experimental standpoint, it is often impractical to measure the environmental parameters that determine the SSP on a dense grid in both time and depth. For example, in long-duration acoustic experiments, high resolution measurements of temperature and salinity are only possible during the deployment and recovery cruises. In the intervening months the environment is sampled by a relatively small number of sensors attached to the acoustic mooring. This paper addresses the problem of using sparse environmental measurements to estimate the SSP with sufficient resolution for mode filter design.

A series of ocean acoustic tomography experiments motivate this work. The series includes the North Pacific Acoustic Laboratory (NPAL) experiment (1998-1999) and the SPICE04/LOAPEX experiment (2004-2005). These experiments employed mode-resolving vertical line arrays (VLA's) to study low-frequency acoustic propagation at megameter ranges. In the NPAL experiment, one of the VLA's was equipped with 10 temperature sensors across its 1400 meter aperture. These sensors logged data at 20-minute intervals during the year-long deployment. Reconstructing a SSP from these measurements is a challenging problem due to the sparseness of the depth sampling and the lack of salinity measurements. The technique described in this paper assumes that the changes in the SSP associated with mesoscale and seasonal effects

can be written in terms of the quasi-geostrophic dynamic modes. The dynamic modes are an orthonormal basis derived from historical oceanographic data for the VLA location. By fitting the observed temperature fluctuations to the dynamic modes, it is possible to obtain an estimate of the SSP required for mode processing. The space-time Kalman filter (STKF) provides a convenient framework for solving the estimation problem. This paper describes the STKF implementation and examines its performance for the NPAL data set. It analyzes the sound speed errors associated with the method and considers how those errors propagate through the mode computations.

The rest of the paper is organized as follows. Section II provides an overview of the NPAL data set used for the analysis and briefly describes the quasi-geostrophic ocean model. Following that, Section III develops the STKF algorithm and a simpler linear least squares algorithm. Section IV demonstrates the performance of these two algorithms, first for a simulated set of test data and then for the measured NPAL data. Section IV concludes the paper.

## II. BACKGROUND

### A. NPAL 1998 Experiment

The data used in this paper are ocean temperature measurements taken in conjunction with the NPAL 1998 billboard array experiment [1]. The experiment took place in the Pacific Ocean off the coast of Pt. Sur, California from July 1998 to July 1999. Five vertical line arrays (VLAs), arranged in a billboard configuration, recorded acoustic receptions from a source off Kauai, Hawaii. One of the five VLAs, located in 1790 meters of water, was fitted with ten temperature sensors located between 197 and 1567 meters in depth. Fig. 1 shows the WOA98 average annual SSP for the experiment location, as well as the vertical locations of temperature sensors and acoustic aperture.

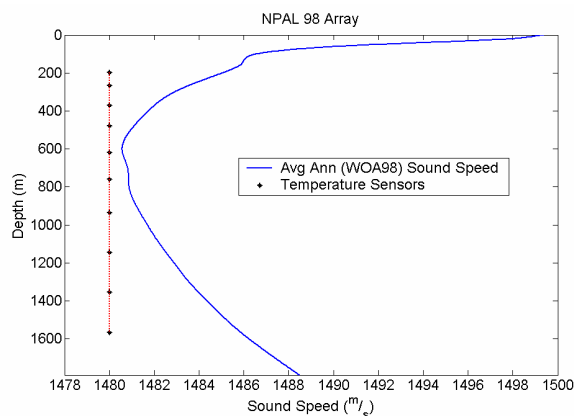


Fig. 1. WOA 98 annual average sound-speed profile and array 5A orientation for NPAL 98 site.

The temperature sensors recorded measurements at

20-minute sampling intervals throughout the experiment. Since the mooring did not include any conductivity sensors, there are no salinity measurements coincident with the temperature time series. Conductivity-temperature-depth (CTD) profiles taken at deployment and recovery provide the only detailed measurements of both the temperature and salinity fields taken in conjunction with the experiment.

### B. Data Set

A subsampled (twelve measurements per day) plot of the recorded time series of temperature measurements is shown in Fig. 2. During the experiment VLA motion was tracked using a long-baseline navigation system. The mooring motion estimates provide a depth time series associated with each temperature sensor. The variances of the depth time series are quite small: the shallowest sensor has a depth variance of 1.3 m, and the remaining sensors have variances of 0.6 m or less. Given these small variances, it is reasonable to assume that each temperature sensor is located at a fixed depth, equal to the average depth obtained from the mooring time series.

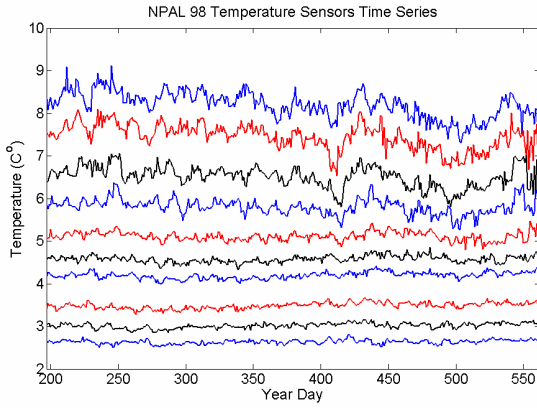


Fig. 2. NPAL 98 measured temperature time series'.

### C. Quasi-Geostrophic Ocean Model

As Fig. 2 indicates, ocean temperature varies significantly over the course of the year-long experiment. This paper assumes that ocean variability (as measured by the temperature fluctuations) is associated with two types of waves: planetary waves and internal waves. These waves occupy different spectral bands. Fluctuations having frequencies less than the inertial frequency are classified as planetary (Rossby) waves, and those having frequencies between the inertial and Brunt-Väisälä frequencies are classified as internal waves [2]. Planetary waves associated with ocean mesoscale fluctuations have periods on the order of 30-60 days, while internal waves have periods on the order of minutes to hours.

The mesoscale fluctuations in a continuously-stratified ocean can be modeled by the QG equations [3]. These fluctuations can be written in terms of a set of normal modes, defined by the Sturm-Liouville problem given below [3, 4]:

$$\begin{aligned} \frac{d}{dz} \left( \frac{1}{N^2(z)} \frac{d\varphi(z)}{dz} \right) + \lambda \varphi(z) &= 0 \\ \frac{d\varphi(z)}{dz} + \frac{N^2(z)}{g} \varphi(z) &= 0; z = 0 \\ \frac{d\varphi(z)}{dz} &= 0; z = -D \end{aligned} \quad (1)$$

$g$  is the gravitational acceleration constant. The normal mode solutions  $\varphi^j(z)$  and eigenvalues  $\lambda_j$  define the planetary (Rossby) wave modes [4]. The planetary wave modes are related to the modes of vertical displacement as follows:

$$\varphi_{\zeta}^j(z) = \frac{1}{N^2(z)} \frac{d\varphi^j(z)}{dz} \quad (2)$$

Equations 3 and 4 define the temperature and sound speed modes associated with the vertical displacement modes:

$$\varphi_T^j = \frac{dT_{pot}(z)}{dz} \varphi_{\zeta}^j(z) \quad (3)$$

$$\varphi_C^j = \frac{dC_{pot}(z)}{dz} \varphi_{\zeta}^j(z) \quad (4)$$

The temperature fluctuations  $\Delta T(z)$  associated with planetary-wave-induced density fluctuations can be written as a sum of the temperature modes:

$$\Delta T_{Rossby}(z) = \sum_j a_j \varphi_T^j(z) \quad (5)$$

where  $a_j$  is the relative weight of each mode. The associated set of sound speed fluctuations can be written as a sum of the sound speed modes:

$$\Delta C_{Rossby}(z) = \sum_j a_j \varphi_C^j(z) \quad (6)$$

It is often assumed that most of the energy in the temperature and sound speed fluctuations can be represented by a relatively small set of modes.

Figures 3 through 5 show the displacement, temperature, and sound speed modes derived using the annual climatology for the NPAL 98 location from the World Ocean Atlas [5, 6]. These modes were obtained by numerical solution of the Sturm-Liouville problem (Eq. 1) in MatLab®. Calculations of buoyancy frequency and potential temperature were implemented using the CSIRO SEAWATER MatLab® library [7]. Spline interpolation was used to compute the basis functions on the one-meter depth grid required by the algorithms described in the next section.

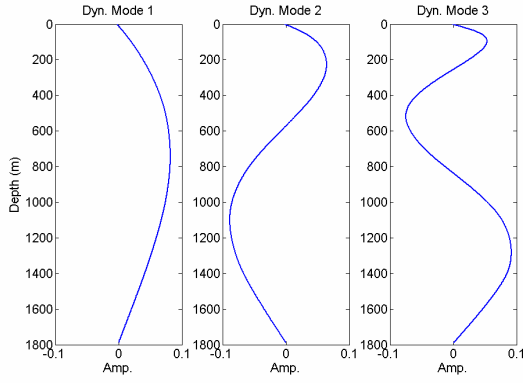


Fig. 3. WOA98 annual average QG Displacement Modes for NPAL 98 location.

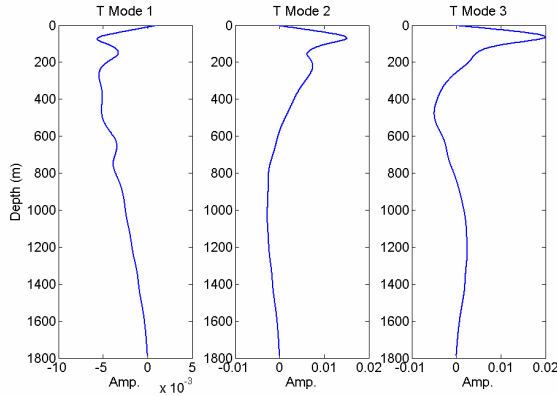


Fig. 4. WOA98 annual average QG Temperature Modes for NPAL 98 location.

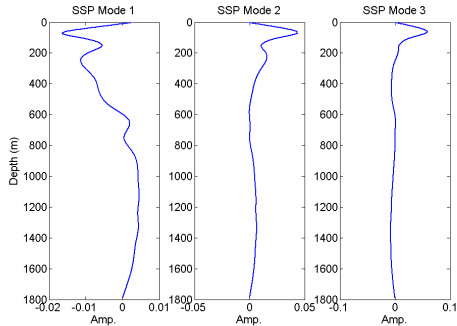


Fig. 5. WOA98 annual average QG Sound Speed Modes for NPAL 98 location.

### III. METHODOLOGY

As noted in the Introduction, knowledge of the sound speed is required in order to design filters for the acoustic normal modes. The sound speed profile at the array can be written:

$$C(t, z) = C_0(z) + \Delta C_{Rossby}(t, z) + \Delta C_{IW}(t, z) \quad (7)$$

where  $C_0(z)$  is the background profile,  $\Delta C_{Rossby}(t, z)$  is the perturbation due to planetary waves and  $\Delta C_{IW}(t, z)$  is the perturbation due to internal waves. This section develops two algorithms for estimating  $C(t, z)$  given measurements of the temperature field at a discrete set of depths along the receiving array. The goal is to track the slow changes in

the SSP due to Rossby waves so that the acoustic mode filter can be updated over time. From this perspective, the sound speed fluctuations due to internal waves represent a noise process that should be filtered out.

Both of the approaches developed below make use of the QG model discussed in the previous section. Although they differ in specifics, both methods use the measured temperatures to infer a time series of expansion coefficients  $a_j(t)$  for the modal representation of the Rossby wave fluctuations (i.e., Equations 5 and 6). Projecting onto the smooth QG mode basis makes it possible to interpolate the temperature profile between the measurement points and to extrapolate the profile outside the depths where measurements are available. Since the modal expansions for temperature and sound speed are linked, estimating the temperature profile automatically provides the desired sound speed estimate.

#### A. Space-Time Kalman Filter Algorithm

The first algorithm is based on a space-time Kalman filter approach developed by Wikle and Cressie [8,9]. The STKF implementation takes the temperature perturbation time series  $\Delta T(t, z)$  as input :

$$\Delta T(t, z) = T_{meas}(t, z) - T_0(z) \quad (8)$$

$T_{meas}$  represents the measured temperature and  $T_0$  is the temperature profile associated with the background sound speed  $C_0$ . Using vector notation to represent the fluctuations at all the temperature sensors, Eq. 8 becomes:

$$\Delta \underline{T}(t) = \underline{T}_{meas}(t) - \underline{T}_0 \quad (9)$$

The presentation of the STKF algorithm given below follows directly from the detailed description given in [8] and [9], however variable names are modified to suit the problem at hand. The application of this algorithm to the problem relies on the assumption that each temperature measurement can be modeled as a smooth process, written as a linear combination of the QG temperature modes, with additive internal wave noise and sensor measurement noise.

$$\Delta \underline{T}(t) = \Phi_T \underline{a}(t) + \underline{v}(t) + \underline{\epsilon}(t) \quad (10)$$

Defining  $\epsilon(z, t)$  as temperature sensor measurement error,  $v(z, t)$  as internal wave-induced temperature fluctuations,  $\Phi_T$  as the matrix of sampled QG temperature modes ( $\Phi_T(z)$ ), and  $\underline{a}(t)$  as the QG mode scaling coefficients, Eq. 10 is the measurement model assumed by the STKF algorithm. This measurement model, along with details provided in [8] and [9], yield the Kalman filter equations

$$\hat{\underline{a}}(t|t) = \hat{\underline{a}}(t|t-1) + G(t)[\Delta \underline{T}(t) - \Phi_T \hat{\underline{a}}(t|t-1)] \quad (11)$$

with mean-squared prediction error

$$P(t|t) = P(t|t-1) - G(t)\Phi_T P(t|t-1) \quad (12)$$

The Kalman gain is given by

$$G(t) = P(t|t-1)\Phi_T' [R + V + \Phi_T P(t|t-1)\Phi_T']^{-1} \quad (13)$$

and one-step-ahead predictions are given by

$$\hat{\underline{a}}(t|t-1) = H\underline{a}(t-1|t-1) \quad (14)$$

$$P(t|t-1) = HP(t-1|t-1)H' + JQJ' \quad (15)$$

The optimal estimates of the smooth QG fluctuations in temperature and sound speed are:

$$\underline{\Delta\hat{T}}(t|t) = \Phi_T \hat{\underline{a}}(t|t) \quad (16)$$

$$\underline{\Delta\hat{C}}(t|t) = \Phi_C \hat{\underline{a}}(t|t)$$

Given these estimates of the Rossby wave fluctuations, the STKF estimate of the sound speed is

$$\underline{\hat{C}}_{STKF}(t) = \underline{C}_0 + \underline{\Delta\hat{C}}(t|t) \quad (17)$$

The  $\Phi_T$  and  $\Phi_C$  matrices are the finely-sampled (one meter interval) QG temperature and sound speed modeshape matrices, respectively.

### B. Linear Least-Squares (LLS) Relationship

The second algorithm is based on a simple linear least squares fit of the temperature modes to the observed temperature fluctuations. The QG coefficients are computed as follows:

$$\hat{\underline{a}}_{LLS}(t) = (\Phi_T' \Phi_T)^{-1} \Phi_T' \underline{\Delta T} \quad (18)$$

Unlike the STKF approach, the LLS method does not provide any temporal smoothing. For comparison to the STKF results, the temperature perturbations  $\Delta T$  must be lowpass-filtered with cutoff at the inertial frequency to remove the internal wave noise.

The detailed estimate of the sound speed profile is then reconstructed as follows:

$$\underline{\hat{C}}_{LLS}(t) = \underline{C}_0 + \Phi_C \hat{\underline{a}}_{LLS}(t) \quad (19)$$

The LLS algorithm is simpler to implement and makes fewer assumptions about the underlying data model.

## IV. RESULTS

Two approaches are considered for evaluating the performance of the STKF algorithm. First, a simple test case is created in which the true QG mode coefficients are known (synthesized) and thus a direct comparison may be made. Second, the STKF results for the NPAL98 data are compared to the results produced by the LLS method presented above.

### A. Test Data

#### i) Construction

A time series of mode coefficients were synthesized and used together with the WOA98 annual average QG temperature and sound speed modes discussed earlier to generate the simulated temperature and sound speed time series. Note that the simulation uses only the first three QG modes. The measurements are taken as the time series at the depths corresponding to the 10 sensors. To

make the simulation more realistic, samples of internal wave noise were added to the simulated measurements. The IW samples were generated by high-pass filtering the observed NPAL98 temperature data (with cutoff at the inertial frequency).

#### ii) Performance

Fig. 6 shows the true QG mode coefficients and the STKF estimates of the coefficients. The Kalman filter tracks the coefficients reasonably well.

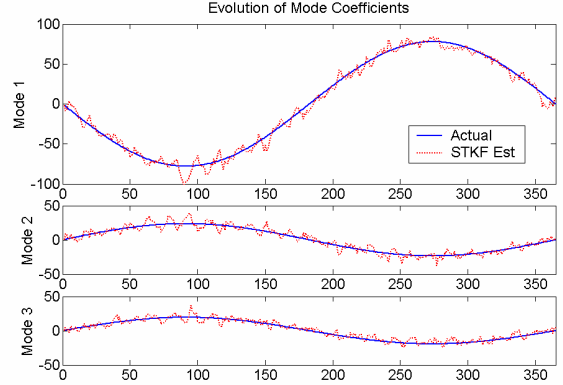


Fig. 6. Test Data true QG mode coefficients and STKF estimates.

Fig. 7 shows the resulting average root mean-squared (RMS) error between the true sound speed and the STKF estimate. The Kalman Filter does very well at depths below the shallowest sensor depth (197 m), which is the area we are most concerned with.

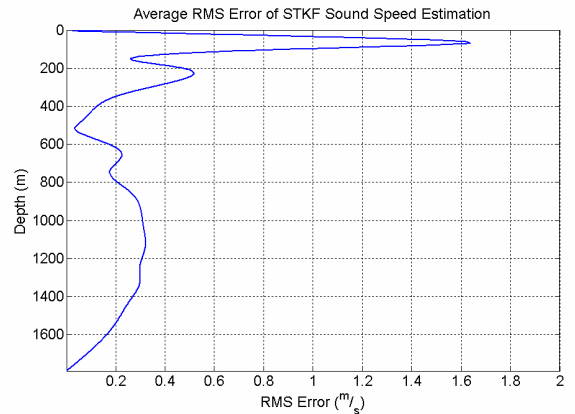


Fig. 7. RMS Error between true simulation sound speed and STKF estimates of sound speed.

The conclusion we may draw from this illustration is that, assuming that the QG ocean model accurately represents the “slower” seasonal and mesoscale fluctuations at a location of interest, then the STKF algorithm we are using is appropriate and will produce reasonable estimates in the presence of internal wave and sensor measurement noise.

### B. NPAL Data Analysis

#### i) Sound Speed Estimates

This section computes sound speed estimates using the NPAL98 temperature measurements. Since the true

underlying SSP is not known for the experimental data, the performance evaluation focuses on comparing the STKF and LLS solutions.

To determine the appropriate number of QG modes to use, the STKF estimates were computed for models that included from one to ten modes. Choosing the right number of modes requires a balance between minimizing complexity and maximizing the quality of fit to the data.

The following fit parameter was used to determine the number of modes to include:

$$\eta = \frac{T'_{est} T_{meas}}{T'_{meas} T_{meas}} \quad (20)$$

Using this parameter, values closest to one denote highest quality fit. Using this method, three modes were chosen as the optimal number to use. Fig. 8 shows a significant improvement occurred between one and three modes. The addition of modes beyond three had a negligible effect.

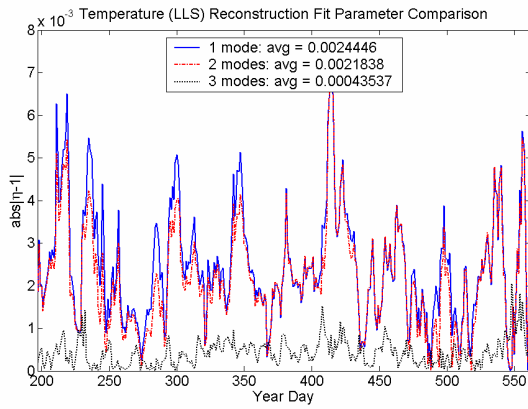


Fig. 8. Quality of fit comparison of NPAL98 data to QG temperature modes.

Using a three-mode model, the NPAL 98 temperature measurements were then processed by the STKF algorithm and the LLS algorithm. Fig. 9 compares the QG mode coefficient estimates produced by the two methods. Fig. 10 shows a plot of average MSE between the resulting sound speed estimates.

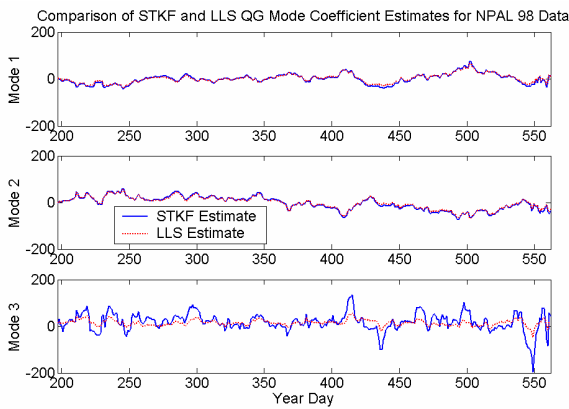


Fig. 9. Comparison of STKF and LLS QG mode coefficient estimates.

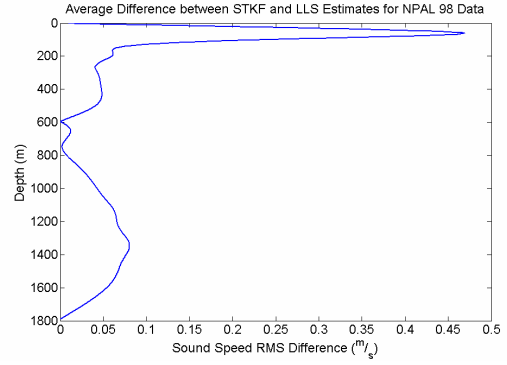


Fig. 10. Average MSE between STKF and LLS sound speed estimates.

The difference in estimates of sound speed by these two methods is relatively small, showing that the STKF method performance is comparable to that of the LLS method.

### ii) Acoustic Mode Estimates

Ultimately we are interested in the effect of the sound speed estimation algorithm on the acoustic modeshape and wavenumber estimates. Acoustic mode estimates were computed using a method of approximation by Chebychev polynomials [10]. Assuming a daily acoustic mode estimate update interval, the sound speed estimates produced by the STKF and LLS methods were averaged over each day of the NPAL experiment and only one acoustic wavenumber and modeshape estimate was computed for each method each day. Fig. 11 shows a comparison of the acoustic wavenumber estimates produced by the STKF and LLS sound speed estimates. Fig. 12 shows a comparison of modeshape estimates for modes 1 and 10, produced by the STKF and LLS sound speed estimates for a representative fifty-day period of the experiment. The modeshapes for the two algorithms are virtually identical. These results demonstrate that both methods produce realistic and similar estimates of acoustic wavenumber and modeshapes. The wavenumber plot indicates that there are particularly strong variations in the mode wavenumbers around yearday 410 and 500. This seems reasonable given the observed fluctuations in the temperature field around these yeardates (see Fig. 2).

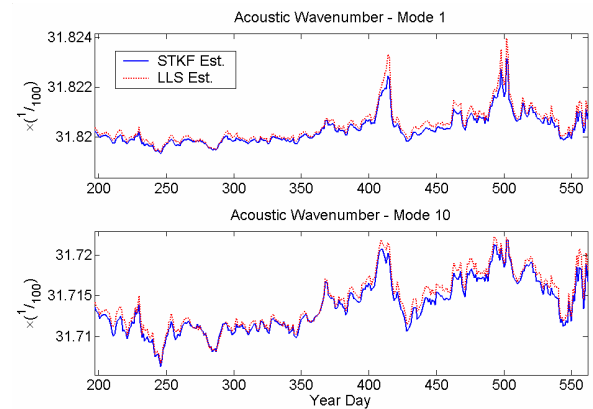


Fig. 11. Comparison of acoustic wavenumber estimates.

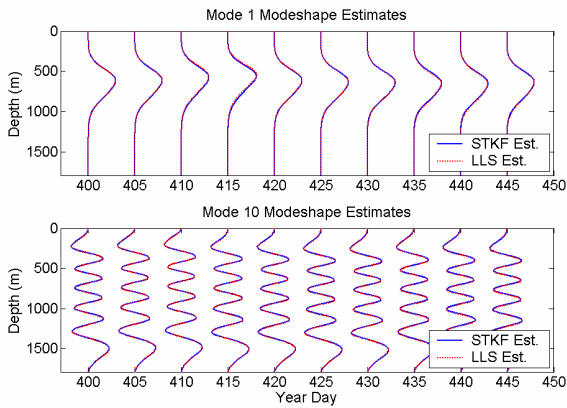


Fig. 12. Comparison of acoustic modeshape estimates.

### iii) Acoustic Mode Filters

It is important to consider how sound speed fluctuations impact acoustic mode estimation. Since mode estimation is a classical linear inverse problem, one of the most common mode filters is the pseudo-inverse (PI) filter, defined as:

$$W' = (E'E)^{-1} E' \quad (21)$$

The matrix E contains the first M columns of the sampled acoustic modeshape matrix. One of the main advantages of the PI filter is that, assuming E is a full-rank matrix, the PI filter is guaranteed to have unity gain in the desired mode and to reject interference from all the other modes included in the filter. The "beampattern" [11] defined as

$$20 \log_{10}(W'E) \quad (22)$$

illustrates this property of the PI filter. The mth row of the beampattern indicates how each of the M modes in the E matrix projects into the estimate for mode m. Fig. 13 shows the beampattern for the 10-mode PI filter designed using the STKF results for yearday 500 of the NPAL98 experiment. The diagonal structure of the beampattern indicates that this PI filter rejects all crosstalk from neighboring modes (up to 10).

Assuming that the PI mode filter is designed with the correct set of modeshapes for the waveguide, it has excellent crosstalk rejection properties. When there is a mismatch between the sampled modeshape matrix used to design the filter and the true modes, the beampattern is no longer guaranteed to have a diagonal structure. For example, Fig. 14 shows the beampattern that results when a PI filter designed using the sound speed measured at array deployment (CTD taken yearday 195) is used to process the modes associated with the measured profile for yearday 500. The highest crosstalk in this figure is on the order of -10 dB. This degree of mismatch severely compromises the ability of the mode filter to resolve the signals propagating in neighboring modes.

Fig. 15 demonstrates how the maximum crosstalk associated with two mode filters varies over the course of the NPAL experiment. The solid blue curve shows the maximum crosstalk for the mode filter designed with the deployment (i.e., CTD) profile. The dashed red curve shows the maximum crosstalk for the mode filter designed using the STKF results for yearday 197. At yearday 197,

the latter filter is perfectly matched with the underlying modes and the mismatch is very small. It is larger for other yeardays due to the variations in the environment. The CTD filter has consistently higher crosstalk due to the mismatch between the modeshapes of the CTD profile and the modeshapes predicted by the STKF algorithm. This plot demonstrates that the PI mode filter needs to be updated over time to avoid crosstalk problems due to sound speed mismatch.

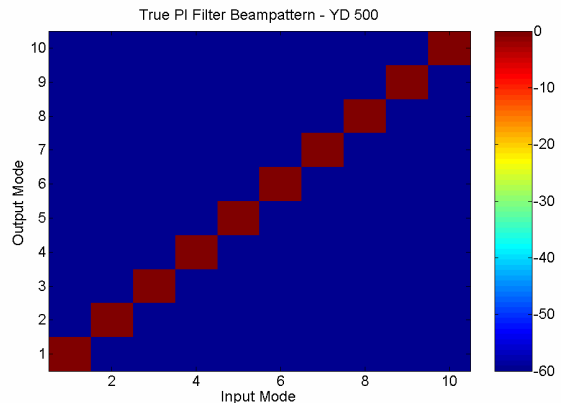


Fig. 13. STKF estimate PI mode filter processing STKF modes for year day 500.

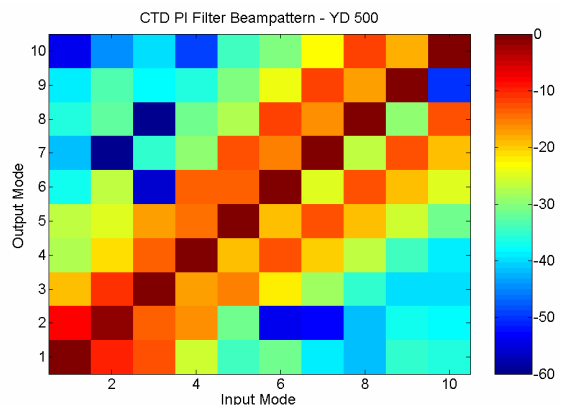


Fig. 14. CTD profile PI mode filter processing STKF modes for year day 500.

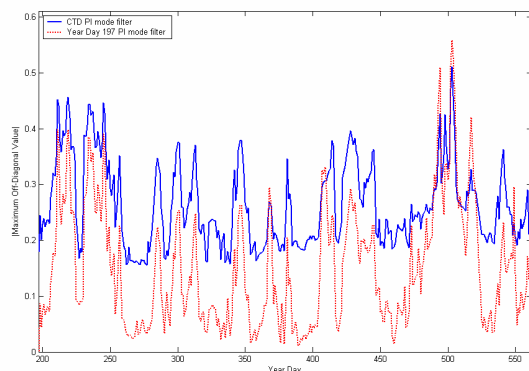


Fig. 15. Maximum crosstalk for CTD profile & Year Day 197 PI mode filters processing STKF mode estimates.

## V. SUMMARY

This paper presented two algorithms for estimating the sound speed profile given samples of the temperature measured along a vertical array. Both the STKF approach and the LLS approach are based on a quasi-geostrophic model for the slow fluctuations associated with planetary waves. After initial testing on a simulated data set, these algorithms were applied to measured data from the NPAL 98 experiment. As the examples in Section IV indicate, both the STKF and LLS methods yield sound speed estimates that translate into reasonable estimates of the acoustic modes. To avoid crosstalk due to environmental mismatch, the acoustic mode filtering for NPAL should be implemented using the time-dependent SSP's produced by one of these algorithms.

## ACKNOWLEDGMENTS

The authors thank Dr. Brian Dushaw (APL-UW) for helpful advice and for sharing his dynamic mode code. This work was supported by an ONR Ocean Acoustics Entry-Level Faculty Award (Grant N00014-02-1-0416). LT Eric St. Pierre worked on this project while completing his master's at George Mason University through the U.S. Coast Guard's postgraduate training program.

## REFERENCES

- [1] Worcester, P.F. and Spindel, R.C., "North Pacific Acoustic Laboratory," *J. Acoust. Soc. Am.*, 117(3), pp. 1499-1510, March 2005.
- [2] Flatte, S.M., Dashen, R., Munk, W., Watson, K. and Zachariassen, F., *Sound Transmission Through a Fluctuating Ocean*, Cambridge University Press, New York, 1979.
- [3] Flierl, G.R., "Models of vertical structure and the calibration of two-layer models", *Dynamics of Atmospheres and Oceans*, 2, 341-381, 1978.
- [4] Howe, B.H. and Worcester, P.F., "Ocean Acoustic Tomography: Mesoscale Velocity", *Journal of Geophysical Research*, 92, 3785-3805, 1987.
- [5] S. Levitus and T. Boyer, *World Ocean Atlas 1994 Volume 4: Temperature*, 1994. NOAA Atlas NESDIS 4, Silver Spring, MD.
- [6] S. Levitus and T. Boyer, *World Ocean Atlas 1994 Volume 3: Salinity*, 1994. NOAA Atlas NESDIS 3, Silver Spring, MD.
- [7] Morgan, P., SEAWATER MatLab® library, version 1.6, CSIRO Division of Oceanography, 1994.
- [8] Wikle, C.K. and Cressie, N., "A dimension-reduced approach to space-time Kalman filtering", *Biometrika*, 86, 815-829, 1999.
- [9] Wikle, C.K. and Cressie, N., "A dimension-reduction approach to space-time Kalman filtering", retrieved March 28, 2005 from <http://www-users.cs.umn.edu/~stello/Wikle-DimensionReduction.pdf>.
- [10] Dzieciuch, M., MatLab aw.m script, Retrieved August 10, 2004 from Ocean Acoustics Library at <http://oalib.saic.com/>.
- [11] K. E. Wage, A. B. Baggeroer, and J. C. Priesig, "Modal analysis of broadband acoustic receptions at 3515-km range in the North Pacific using short-time Fourier techniques," *J. Acoust. Soc. Am.* 113, 801-817, 2003.